Doped Manganites Phase Diagram from a Continuum Double Exchange Model

José María Román

Loomis Laboratory of Physics, University of Illinois at Urbana-Champaign,
1110 W. Green St., Urbana, IL 61801-3080, USA.

Joan Soto

Dpt. d'Estructura i Constituents de la Matèria, Universitat de Barcelona,
Av. Diagonal 647, E-08028, Barcelona, Spain.

August 16th, 1999

We present a continuum model for doped manganites which consist of two species of quantum spin 1/2 fermions interacting with classical spin fields. The phase structure at zero temperature turns out to be considerably rich: antiferromagnetic insulator, antiferromagnetic two band conducting, canted two band conducting, canted one band conducting and ferromagnetic one band conducting phases are identified, all of them being stable against phase separation. There are also regions in the phase diagram where phase separation occurs.

Doped Manganites

The manganites are a generic group of alloys which present a rich magnetic structure in their ground state, from antiferromagnetism to ferromagnetism going through canted phases (i.e., the magnetisations in the even and odd sublattices form an angle θ, $0 < \theta < \pi$) or phase separation regions [1, 2, 3, 4, 5].

General Formula: $La_{1-x}A_xMnO_3$, $A = Ca, Sr, Ba$, and $0 \leq x \leq 1$ represents the number of La atoms substituted by type A atoms. The valence of the different elements is La^{3+}, A^{2+}, Mn^{3+} ($[Ar]3d^4$) or Mn^{4+} ($[Ar]3d^3$) and O^{2-}. Therefore, each substitution $La^{3+} \rightarrow A^{2+}$ corresponds to a substitution in the manganese atom $Mn^{3+} \rightarrow Mn^{4+}$.

Crystallographic Structure: Manganites crystalise in a Perovskite distorted structure, with the Mn atoms at the vertices of a cube, the other metallic elements (La, Ca, Sr, Ba) body centered in the cube, and the O in the middle of the edges. This ideal cubic structure is slightly distorted to an orthorhombic structure by the Jahn-Teller distortion.

Electronic Structure: The crystalline field splits the 5-fold $3d$-bands into a 3-fold t_{2g}-band and a 2-fold e_g-band. For small x (doping) an additional structural distortion (Jahn-Teller distortion) produces a further splitting of the 2-fold e_g-band.

Magnetic Structure: In this situation the extreme compounds, i.e., $LaMnO_3$ ($x = 0$) and $AMnO_3$ ($x = 1$) behave like semiconductors with an AF ground state. On the other hand, for $0.2 < x < 0.4$ a F ground state with conducting properties is observed.

These properties suggest that the magnetic and electronic properties are related. Indeed, Zener in his Double Exchange Model [2] postulates that the exchange of the electrons from Mn^{3+} to Mn^{4+} atoms through the O atoms produces a lowering in the energy of the system, and since these exchanges do not modify the spin of the electrons the most favored state is the ferromagnetic one.

Continuum Double Exchange Model

The low energy and momentum properties of the system can be studied from a continuum model, where the fields representing the excitations are slowly varying in the space and time.

A Background Magnetisation is generated by the core spins in the t_{2g}-band, and is considered classical. Because of the AF configuration is impossible to describe the magnetic structure with only one slowly varying magnetisation field. Therefore, two slowly varying magnetisation fields are introduced, $\mathbf{M}_1(x)$ and $\mathbf{M}_2(x)$, associated to the even and odd sublattices in the crystal.

Charged Carriers correspond to the holes generated in the e_g-band as the doping increases. These conducting holes are described by two slowly varying fermionic fields, $\psi_1(x)$ and $\psi_2(x)$, which interact locally (Hund coupling) with the corresponding magnetisation. The hopping between the two sublattices is introduced by considering an exchange beetwen the fermionic fields with an amplitude t.

The **continuum double-exchange model** is described by the lagrangian

$$\begin{aligned}\mathcal{L}(x) \;=\; & \psi_1^\dagger(x)\left[(1+i\epsilon)i\partial_0 + \frac{\partial_i^2}{2m} + \mu + J_H\frac{\boldsymbol{\sigma}}{2}\mathbf{M}_1(x)\right]\psi_1(x) \\ & + \psi_2^\dagger(x)\left[(1+i\epsilon)i\partial_0 + \frac{\partial_i^2}{2m} + \mu + J_H\frac{\boldsymbol{\sigma}}{2}\mathbf{M}_2(x)\right]\psi_2(x) \\ & + t\left(\psi_1^\dagger(x)\psi_2(x) + \psi_2^\dagger(x)\psi_2(x)\right) - J_{AF}\mathbf{M}_1(x)\mathbf{M}_2(x).\end{aligned}$$

The size of the parameters in the model are estimated by comparation with the naïve continuum limit of lattice double exchange models. For a cubic lattice we have $2m \sim 1/a^2t^l$, $t \sim zt^l$, $J_H \sim J_H^l$ and $J_{AF} \sim zJ_{AF}^l/a^3 > 0$, where a is the lattice spacing, $z = 6$ is the coordination number and the superscript l means the analogous lattice quantity.

Model restriction: The number of doping holes is controlled by the chemical potential. Since the system is insulator at $t = 0$ the chemical potential must lie bellow the lowest band for $t = 0$, namely, $t < -|J_H|M/2$.

Effective Potential: Phase Diagram

By considering that the ground state configuration is constant, the integration of the fermionic fields in the path-integral yields an effective potential for the ground state in terms of $y = \cos(\theta/2)$ (θ is the angle between $\mathbf{M}_1$ and $\mathbf{M}_2$).

The restriction of the chemical potential ensures that only the two lowest bands contribute to the effective potential, which motivates the reparametrization of the chemical potential

$$\Omega_\pm = -\frac{|J_H|M}{2}\sqrt{1+\gamma^2 \pm 2\gamma y} - \mu \quad , \quad \gamma \equiv \frac{2t}{|J_H|M}$$

$$\mu = -\frac{|J_H|M}{2}\sqrt{1+\gamma^2 - 2\gamma y_0} \qquad (-1 < y_0 < y_0^{max} = \gamma/2).$$

In doped manganites $t \ll J_H$, i.e., $\gamma \ll 1$. In this approximation we obtain the **effective potential**

$$V_{eff} = V_0\left[(2y^2-1) - A\left((y_0+y)^{5/2}\theta(y_0+y) + (y_0-y)^{5/2}\theta(y_0-y)\right)\right]$$

$$V_0 = J_{AF}M^2 \qquad , \qquad A = \frac{(2m)^{3/2}\,t^{5/2}}{15\pi^2 J_{AF}M^2} = \frac{z^{3/2}}{15\pi^2}\,\frac{t}{(J_{AF}a^3M^2)}.$$

The phase diagram arises from the minimisation with respect to y. We obtain antiferromagnetic ($y = 0$, $AFI, AFC2$), canted ($0 < y < 1$, $CC1, CC2$) and F ($y = 1$, $FC1$) phases. In each case the phases can be insulating (I) or conducting (C) with 1 or 2 bands.

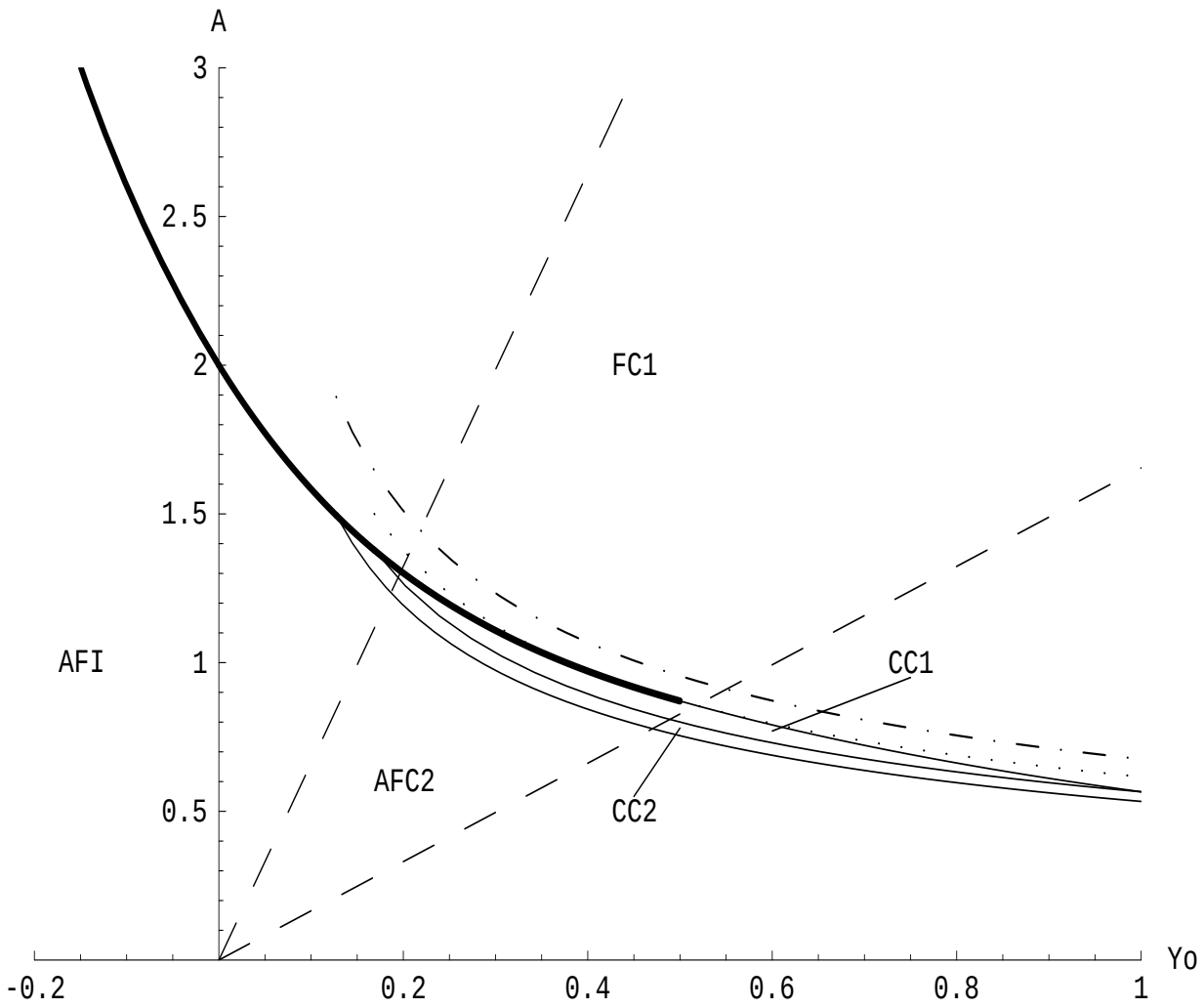

Figure 1: Phase diagram in the (y_0, A) plane. The thick solid line corresponds to first order transitions whereas the remaining solid lines to second order ones. The dotted and dashed dotted lines are the upper stability boundaries for the CC1 and CC2 phases respectively. The two dashed lines are the boundaries for the reliability of our model for $z|J_H|M/2(J_{AF}a^3M^2) \sim 50$ and $z|J_H|M/2(J_{AF}a^3M^2) \sim 200$ respectively. Only the part of the phase diagram to the left of the corresponding dashed line is trustworthy in each case.

- Our model restricts the values of the chemical potential to $y_0 < y_0^{max} = \gamma/2$. By substituting this expression in A we obtain the validity region for the phase diagram

$$A \; > \; \frac{2z^{1/2}}{15\pi^2} \, \frac{z|J_H|M}{2(J_{AF}a^3M^2)} \, y_0^{max}.$$

  It turns out to be a straight line in fig. 1 provided that J_{AF} and J_H remains constant as y_0^{max} varies.

- Fig. 1 plots a phase diagram against the chemical potential, y_0, rather than the number of conducting fermions or doping, x. Since V_{eff} is to be regarded as a (zero temperature) grand canonical potential the doping is introduced via

$$x \; = \; -a^3 \, \frac{\partial V_{eff}}{\partial \mu} \; = \; -\frac{a^3}{t} \, \frac{\partial V_{eff}}{\partial y_0}.$$

- The values for the coupling constants are $t/(J_{AF}a^3M^2) \sim 10 - 20$ and $z|J_H|M/2(J_{AF}a^3M^2) \sim 50 - 200$, which is compatible with the values given in the literature. For these values $A \sim 1 - 2$, and the two extreme validity curves are displayed as dashed lines in fig. 1 and fig. 2.

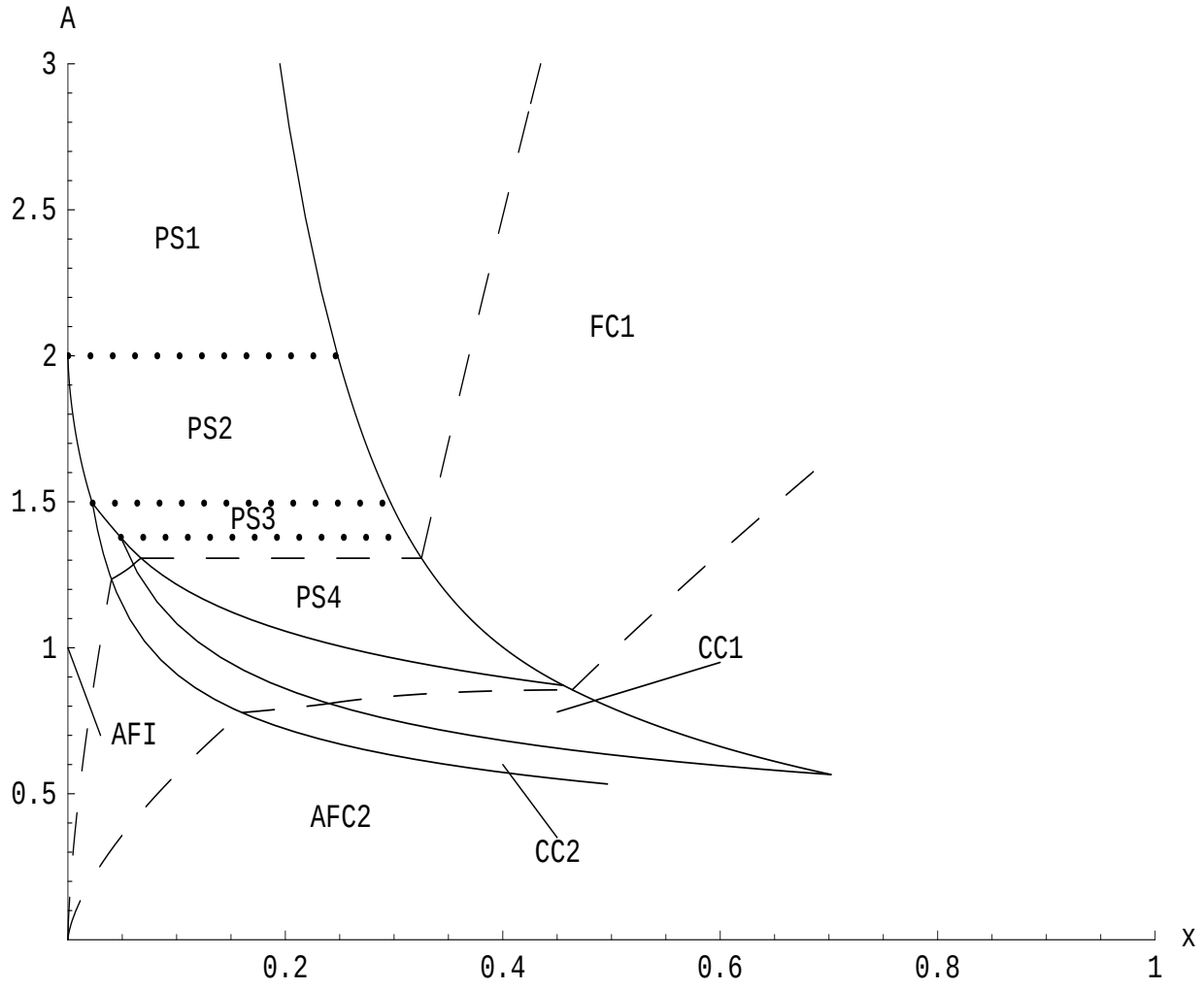

Figure 2: Phase diagram in the (x, A) plane. PSi $(i = 1, 2, 3, 4)$ indicates the new regions where the phases at their boundary may coexist. The $x = 0$ axis corresponds to the AFI phase. The two dashed lines are the boundaries for the reliability of our model for $z|J_H|M/2(J_{AF}a^3M^2) \sim 50$ and $z|J_H|M/2(J_{AF}a^3M^2) \sim 200$ respectively. Only the part of the phase diagram to the left of the corresponding dashed line is trustworthy in each case.

Conclusions

- We have presented a simple model in the continuum which is able to describe the rich phase structure of doped manganites for a wide range of these materials.

- The phase diagram presents the following phases:

  AFI: Antiferromagnetic Insulator

  AFC2: Antiferromagnetic Conductor (2-bands)

  CC2: Canted Conductor (2-bands)

  CC1: Canted Conductor (1-band)

  FC1: Ferromagnetic Conductor (1-band)

  PSi: Phase Separation regions

- The canted phases are thermodynamically stable.

- For realistic values of the parameters, $A \sim 1-2$ ($A \sim t/J_{AF}$), the system can undergo several phase transitions as the doping, x, increases (compare with [6, 7, 8, 9, 10, 11, 12, 13, 14]).

  (i) $AFI - PS1 - FC1$

  (ii) $AFI - AFC2 - PS2 - FC1$

  (iii) $AFI - AFC2 - CC2 - PS3 - FC1$

  (iv) $AFI - AFC2 - CC2 - CC1 - PS4 - FC1$

References

[1] G. H. Jonker and J. H. Van Santen, *Physica* **50** (1950) 337.

[2] C. Zener, *Phys. Rev.* **82** (1951) 403.

[3] P. W. Anderson and H. Hasegawa, *Phys. Rev.* **100** (1955) 675.

[4] P. G. De Gennes, *Phys. Rev.* **118** (1960) 141.

[5] A. P. Ramirez, *J. Phys.: Cond. Matter* **9** (1997) 8171.

[6] D. P. Arovas and F. Guinea, *Phys. Rev.* **B58** (1998) 9150;

[7] D. P. Arovas, G. Gómez-Santos and F. Guinea, *Phys. Rev.* **B59** (1999) 13569.

[8] M. Yu Kagan, D. I. Khomskii and M. Mostovoy, *Canted Spin or Phase Separation in the Double-Exchange Model*, cond-mat/9804213.

[9] L.-J. Zou, Q.-Q. Zheng and H. Q. Liu, *Phys. Rev.* **B56** (1997) 13669.

[10] A. J. Millis, P. B. Littlewood and B. I. Shraiman, *Phys. Rev. Lett.* **75** (1995) 5144.

[11] R. Maezono, S. Ishihara and N. Nagaosa, *Phys. Rev.* **B58** (1998) 11583.

[12] D. I. Golosov, M. R. Norman and K. Levin, *Phys. Rev.* **B58** (1998) 8617.

[13] S. Yunoki, A. Moreo and E. Dagotto, *Phys. Rev. Lett.* **81** (1998) 5612;

E. Dagotto, S. Yunoki and A. Moreo, *Phase separation in models for manganites: theoretical aspects and comparation with experiments*, cond-mat/9809380.

[14] J. W. Lynn *et al.*, *Phys. Rev. Lett.* **76** (1996) 4046;

Y. Yamada *et al.*, *Phys. Rev. Lett.* **77** (1996) 904;

G. Allodi *et al.*,*Phys. Rev.* **B56** (1997) 6036;

J. M. De Teresa *et al.*, *Phys. Rev.* **B57** (1998) 3305;

M. Hennion *et al.*, *Phys. Rev. Lett.* **81** (1998) 1957;

Wei Bao *et al.*, *Solid State Comm.* **98** (1996) 55.

[15] J.M. Román and J. Soto, *Phys. Rev.* **B59** (1999) 11418;

J.M. Román and J. Soto, *Spin Waves in Canted Phases*, in preparation, prepint no. UB-ECM-PF 98/19.